Journal of Advanced Ceramics
2016, **5**(2): 159–166
DOI: 10.1007/s40145-016-0185-1

ISSN 2226-4108
CN 10-1154/TQ

Research Article

Dielectric properties of $(Zn)_x$/CuTl-1223 nanoparticle–superconductor composites

M. MUMTAZ[a,*], Liaqat ALI[a], Shoaib AZEEM[a], Saad ULLAH[a], G. HUSSAIN[a], M. W. RABBANI[a], Abdul JABBAR[b], K. NADEEM[a]

[a]*Materials Research Laboratory*, *Department of Physics*, *FBAS*, *International Islamic University* (*IIU*), *Islamabad 44000*, *Pakistan*
[b]*Department of Physics*, *Ghazi University*, *Dera Ghazi Khan 32200*, *Pakistan*

Received: January 25, 2016; Revised: March 11, 2016; Accepted: March 16, 2016

Abstract: Zinc (Zn) nanoparticles and $(Cu_{0.5}Tl_{0.5})Ba_2Ca_2Cu_3O_{10-\delta}$ (CuTl-1223) superconducting phase were prepared separately by sol–gel and solid-state reaction methods, respectively. Zn nanoparticles were added in CuTl-1223 superconducting matrix with different weight percentage during the final sintering process to obtain $(Zn)_x$/CuTl-1223 (x = 0–4 wt%) nanoparticle–superconductor composites. The effect of Zn nanoparticles on structural, morphological, superconducting, and dielectric properties of CuTl-1223 phase was investigated. The addition of these Zn nanoparticles has not affected the crystal structure of host CuTl-1223 superconducting phase. Superconducting properties were enhanced after the addition of Zn nanoparticles up to certain optimum content (i.e., x = 1 wt%), which were due to improved inter-grain connectivity by healing up of micro-cracks and reduction of defects like oxygen deficiencies, etc. The activation energy (U) was increased after the addition of Zn nanoparticles in CuTl-1223 phase. The dielectric properties of these samples (i.e., dielectric constant, dielectric loss) were determined by experimentally measured capacitance (C) and conductance (G) as a function of frequency at room temperature. The addition of metallic Zn nanoparticles in CuTl-1223 matrix has overall suppressed the dielectric parameters of $(Zn)_x$/CuTl-1223 nanoparticle–superconductor composites. The metallic Zn nanoparticles played a significant role in inter-grain couplings by filling the voids and pores.

Keywords: $(Zn)_x$/CuTl-1223 nanoparticle–superconductor composites; dielectric properties; activation energy

1 Introduction

One of the most eminent phase of $(Cu_{1-x}Tl_x)Ba_2Ca_{n-1}Cu_nO_{2n+4-\delta}$ (n = 2, 3, 4, ⋯) high temperature superconducting family is $(Cu_{0.5}Tl_{0.5})Ba_2Ca_2Cu_3O_{10-\delta}$ (CuTl-1223) [1]. CuTl-1223 superconducting phase has long coherence length along c-axis (ξ_c) [2], low superconducting anisotropy ($\gamma = \xi_{ab}/\xi_c$) [3], small penetration depth (λ), high zero resistivity critical temperature ($T_c(0)$), high irreversibility field (H_{irr}), and high critical current density (J_c) [4,5]. The performance of bulk high temperature superconductors can be severely affected by inter-grain voids, micro-cracks, and pores [6–8]. Different strategies have been exercised to minimize the voids and pores in

* Corresponding author.
E-mail: mmumtaz75@yahoo.com

CuTl-1223 phase [9,10]. Here, we have implemented an easy, effective, and innovative technique of the addition of Zn nanoparticles in CuTl-1223 superconducting matrix. The places, where these nanoparticles reside are only the voids and grain boundaries or grain surfaces. The key objective of this research is the progression of inter-grain connectivity and to scrutinize its effects on superconductivity and dielectric properties of $(Zn)_x$/CuTl-1223 nanoparticle–superconductor composites.

In CuTl-1223 phase, the charge reservoir layer $(Cu_{0.5}Tl_{0.5})Ba_2O_{4-\delta}$ consists of Tl^{3+}, Cu^{2+}, and Ba^{2+} ions, which can localize the charge carriers, while the conducting CuO_2 plane consists of mobile charge carriers. The dielectric constant ascends from the accretion of carriers in between $(Cu_{0.5}Tl_{0.5})Ba_2O_{4-\delta}$ charge reservoir layer and CuO_2 plane [11,12]. The charge reservoir layer, inter-grain boundaries, and micro-cracks act as dielectric media, which can be polarized by the displacement of charge carriers with the assistance of an external electric field from their equilibrium position. The material may undergo four primary mechanisms of polarization [13–16] each of which involves a short-range motion of charges and subsidizes to the total polarization of the material:

- Electronic polarization (α_e). It arises when shifting of electronic charge clouds of atoms and ions takes place. This is observed at very high frequencies such as 10^{16} Hz, i.e., in ultra violet optical region.
- Lattice polarization (α_a). The origin of this polarization is the combined displacement of ion cores and their electronic charge distribution. This is observed at frequencies ranging from 10^{10} to 10^{13} Hz, i.e., in infrared optical region.
- Dipolar polarization (α_0). It originates from the permanent dipoles or from the presence of charge carriers, which is active at lower frequencies from 10^3 to 10^6 Hz, i.e., in the sub-infrared optical region due to their longer relaxation time.
- Interfacial polarization (α_i). This polarization is sensitive at low frequency range of 10^3 Hz and may extend to a few kHz [6,13,17].

Dielectric properties of $Cu_{0.25}Tl_{0.75}Ba_2Ca_3Cu_4O_{12-\delta}$ superconductor with addition of MgO nanoparticles were investigated in frequency range from 100 Hz to 4 MHz [7]. Volume fraction and connectivity between grains were found to be increased by the addition of these nanoparticles by healing micro-cracks. Increase in ε_r' and decrease in σ_{ac} were observed up to certain optimum level of the nanoparticle content. Dielectric constants (ε_r', ε_r'') and dielectric loss ($\tan\delta$) of Tl-based high temperature superconductors (HTSCs) were found to depend strongly on operating temperature and frequency of external applied ac-field [6]. Negative capacitance (NC) phenomenon was observed in $Cu_{0.5}Tl_{0.5}Ba_2Ca_3Cu_{4-y}Zn_yO_{12-\delta}$ ($y = 0, 3$) superconductor at different frequencies and temperature [13,18]. Effect of oxygen post-annealing on superconductivity and dielectric properties of $Cu_{0.5}Tl_{0.5}Ba_2Ca_3(Cu_{4-y}Cd_y)O_{12-\delta}$ was investigated [19]. A strong dielectric dispersion was observed at low frequencies and temperature, while reverse effects were observed at high temperature and frequencies. The dielectric constant determines the nature of the superconducting material, i.e., the binding forces to which the mobile carriers are tied among the conducting CuO_2 planes and $Cu_{0.5}Tl_{0.5}Ba_2O_{4-\delta}$ charge reservoir layers. The real part of the dielectric constant (ε') shows energy stored within the material when exposed to electric field. The imaginary part of the dielectric constant (ε'') indicates the absorption and the attenuation of energy across the interfaces under an external electric field. Electrical nature of materials can be described by dielectric properties. Materials with high dielectric constant are used in micro-electronic devices. In this article, we reported the frequency-dependent dielectric measurements for $(Zn)_x$/CuTl-1223 nanoparticle–superconductor composites. Different parameters related to dielectric measurements like dielectric constant (both real and imaginary parts), tangent loss, and ac-conductivity have been calculated in the frequency range of 10^{-1} to 10^7 Hz at room temperature, i.e., 293 K.

2 Experimental details

$(Zn)_x$/CuTl-1223 nanoparticle–superconducting composites were synthesized by using solid-state reaction method. Initially Cu(CN), $Ba(NO_3)_2$, and $Ca(NO_3)_2$ compounds were mixed in appropriate ratios to prepare bulk $Cu_{0.5}Ba_2Ca_2Cu_3O_{10-\delta}$ precursor material. The mixed material was ground in agate mortar and pestle for 2 h. After grinding, the mixed material was loaded in quartz boat and fired at 860 ℃ for 24 h in pre-heated chamber furnace followed by furnace cooling to room temperature. The firing step was repeated after 2 h grinding under the same conditions.

The calculated amounts of Tl_2O_3 and Zn nanoparticles were mixed in $Cu_{0.5}Ba_2Ca_2Cu_3O_{10-\delta}$ precursor material. The mixed material obtained was pelletized under 3.8 tons/cm^2 pressure by using hydraulic press [20,21]. The pellets were wrapped in gold capsules (to avoid Tl leakage) and sintered for 10 min at 860 ℃ in pre-heated chamber furnace followed by quenching to room temperature in order to obtain the final product $(Zn)_x$/CuTl-1223 (x = 0–4 wt%) nanoparticle–superconductor composites.

These composites were characterized by X-ray diffraction (XRD), scanning electron microscopy (SEM), temperature-dependent resistance measurements, and dielectric properties. The structural phases of nanoparticles and composites were determined by XRD. The average size of nanoparticles was calculated by using Debye–Scherrer's formula. The cell parameters were determined by using Check Cell computer software. The surface morphology and chemical composition were examined by SEM and energy dispersive X-ray (EDX) analysis, respectively. Conventional four-probe method was used to measure temperature-dependent resistance of these samples. The frequency-dependent dielectric measurements were carried out by using an LCR meter at frequencies from 10^{-1} to 10^7 Hz. Typical two-probe technique was used for frequency-dependent dielectric measurements. Silver paint was applied to both the surfaces and was dried at room temperature. By measuring the conductance (G) and capacitance (C), the dielectric constant (ε_r), dielectric loss ($\tan\delta$), and ac-conductivity (σ_{ac}) of the samples were determined by using following equations [13,20]:

$$\varepsilon_r = \frac{\varepsilon_m}{\varepsilon_0} \tag{1}$$

$$\varepsilon' = \frac{Cd}{\varepsilon_0 A} \tag{2}$$

$$\varepsilon'' = \frac{Gd}{\varepsilon_0 A\omega} \tag{3}$$

$$\tan\delta = \frac{\varepsilon''}{\varepsilon'} \tag{4}$$

$$\sigma_{ac} = \omega\varepsilon'\varepsilon_0 \tan\delta \tag{5}$$

where d is the thickness of pellets, A is the area of electrode, G is the conductance, $\omega = 2\pi f$ is the angular frequency, f is the frequency of applied ac-field, ε_m is the permittivity of material, ε_0 is the permittivity of free space, and ε_r is the relative permittivity.

3 Results and discussion

XRD spectrum exhibits prominent sharp diffraction peaks indexed with hexagonal structure of Zn nanoparticles as shown in Fig. 1. XRD analysis shows the distinct diffraction peaks at 2θ = 36.34°, 39.06°, 43.28°, 54.36°, which are indexed to (002), (010), (011), and (012) planes, respectively. The hexagonal structure of Zn nanoparticles matches well with the database of JCPDS, indicating that Zn nanoparticles have crystalline structure. The average size of Zn nanoparticles calculated by Debye–Scherrer's formula is 50 nm. No prominent peak of impurity is found in XRD spectrum of Zn nanoparticles. The XRD spectra of $(Zn)_x$/CuTl-1223 nanoparticle–superconducting composites with different weight percentage of Zn nanoparticles (i.e., x = 0–4 wt%) are shown in Fig. 2. Most of the diffraction peaks are well indexed in accordance to CuTl-1223 tetragonal structure, following *P*4/*mmm* space group. These peaks correspond to CuTl-1223 phase with lattice parameters a = 4.01 Å,

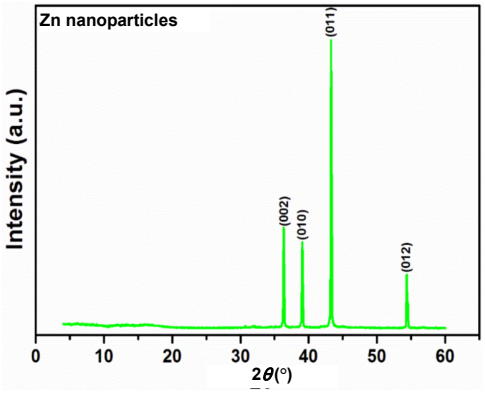

Fig. 1 XRD spectrum of Zn nanoparticles.

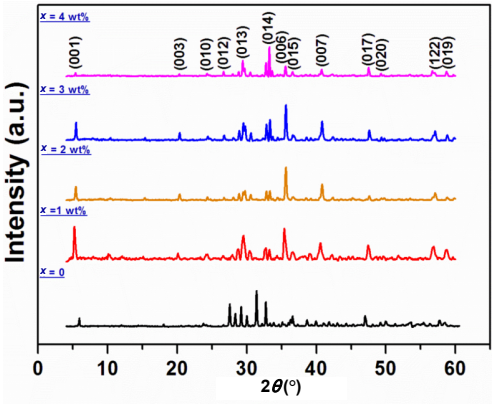

Fig. 2 XRD spectra of $(Zn)_x$/CuTl-1223 nanoparticle–superconductor composites with x = 0–4 wt%.

$c = 14.95$ Å for $x = 0$; $a = 3.03$ Å, $c = 15.85$ Å for $x = 1$ wt%; $a = 3.77$ Å, $c = 15.25$ Å for $x = 2$ wt%; $a = 3.70$ Å, $c = 15.20$ Å for $x = 3$ wt%; and $a = 3.70$ Å, $c = 15.48$ Å for $x = 4$ wt%. A few un-indexed peaks of low intensity also appear, which are possibly due to presence of impurities or some other superconducting phases. A slight shift of the diffraction peaks to lower angles is observed, which may be due to strains produced in the material after the addition of Zn nanoparticles. Figure 3 shows SEM images of $(Zn)_x$/CuTl-1223 nanoparticle–superconductor composites with $x = 0, 2$ wt%. High porosity, weak inter-grain connectivity, and disorientation of grains in pure CuTl-1223 superconducting phase can be visualized in Fig. 3(a). Inter-grain connectivity and improved grain size after addition of Zn nanoparticles in CuTl-1223 superconducting matrix can be seen in Fig. 3(b). The improvement in inter-grain connections and grain size may be due to healing up of inter-grain voids after inclusion of metallic Zn nanoparticles. EDX spectra of $(Zn)_x$/CuTl-1223 nanoparticle–superconductor composites ($x = 2$, 4 wt%) are shown in Fig. 4, which show the presence of different elements in the composites. XRD, SEM, and EDX show that Zn nanoparticles occupy the interstitial spaces between the grains and do not affect the crystal structure of host CuTl-1223 phase. The temperature-dependent resistance measurements of $(Zn)_x$/CuTl-1223 nanoparticle–superconductor composites ($x = 0$, 1, 3 wt%) are shown in Fig. 5. The metallic variation in resistance from room temperature down to onset of superconductivity with critical temperature $T_c(0)$ around 92, 101, and 100 K for $x = 0$, 1, 3 wt% has been observed, respectively.

These measurements indicate the increase in critical temperature $T_c(0)$ from 92 to 101 K after the addition of 1 wt% of Zn nanoparticles. The increase in $T_c(0)$ is due to the facilitation of mobile free carriers and improvement in the inter-grain connectivity after addition of Zn nanoparticles in CuTl-1223 phase. The initial rise in $T_c(0)$ is due to increase in superconducting volume fraction and improved weak-links after the addition of Zn nanoparticles at the grain boundaries of CuTl-1223 matrix.

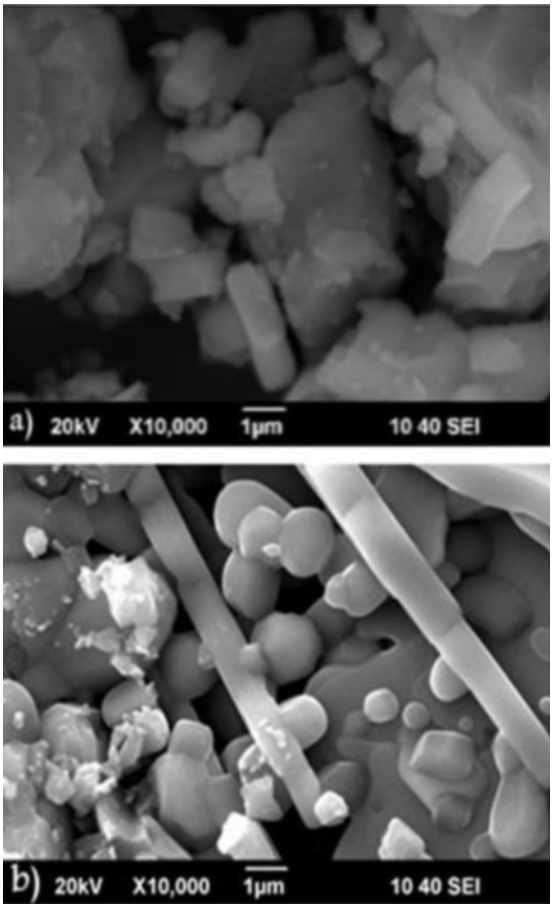

Fig. 3 SEM images of $(Zn)_x$/CuTl-1223 nanoparticle–superconductor composites with (a) $x = 0$ and (b) $x = 2$ wt%.

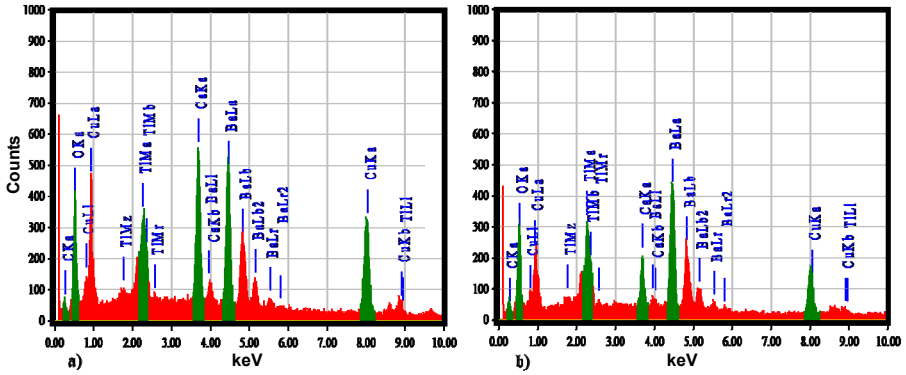

Fig. 4 EDX spectra of $(Zn)_x$/CuTl-1223 nanoparticle–superconductor composites with (a) $x = 2$ wt% and (b) $x = 4$ wt%.

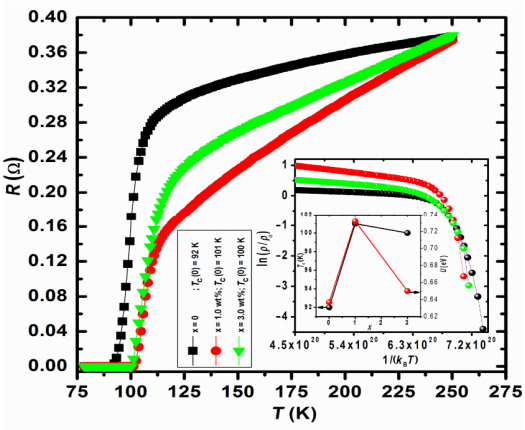

Fig. 5 Resistance versus temperature measurements of $(Zn)_x$/CuTl-1223 nanoparticle–superconductor composites with $x = 0$, 1, 3 wt%. In the inset, there are shown the Arrhenius plots and variation of T_c and U as a function of Zn nanoparticle content (i.e., $x = 0$, 1, 3 wt%).

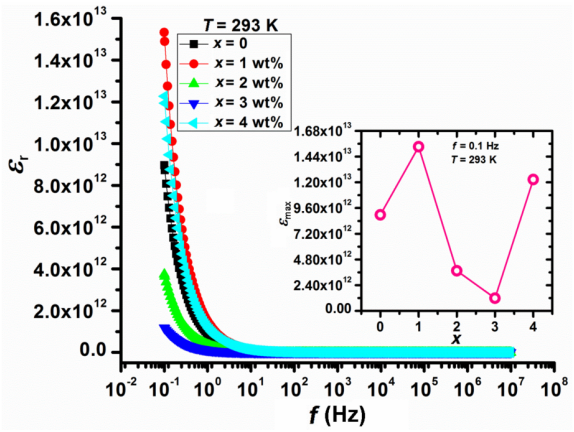

Fig. 6 Variation of dielectric constant (ε_r) of $(Zn)_x$/CuTl-1223 nanoparticle–superconductor composites versus frequency for $x = 0$–4 wt%. In the inset, there are shown the variation of maximum ε_r versus Zn nanoparticle content (i.e., x).

The dipolar polarization relaxation time obeys the Arrhenius equation according to the Debye model, which is

$$\frac{\rho}{\rho_0} = \frac{U}{k_B T} \tag{6}$$

where U is the activation energy; k_B is the Boltzmann constant; and ρ_0 is the normal state resistivity. The plot of $\ln(\rho/\rho_0)$ versus $1/(k_B T)$ showing the activated behavior is given in the inset of Fig. 5. To calculate the activation energy, the region close to superconducting transition is chosen and it is observed that the activation energy is increased after the addition of Zn nanoparticles in CuTl-1223 matrix. The maximum value of activation energy is found in the sample with $x = 1$ wt%. The increase of activation energy may be due to interaction of carriers with the metallic Zn nanoparticles at grain boundaries.

Dielectric properties of $(Zn)_x$/CuTl-1223 nanoparticle–superconductor composites with $x = 0$–4 wt% have also been examined. The variation in frequency-dependent dielectric constant (ε_r) of the samples at room temperature is shown in Fig. 6. The dielectric constant is decreased with increase of frequency. The carriers can not follow the frequency of external applied electric ac-field at high frequencies and dielectric response becomes ineffective. The maximum values of ε_r at frequency 10^{-1} Hz are found around 8.96×10^{12}, 1.53×10^{13}, 3.74×10^{12}, 1.181×10^{12}, and 1.22×10^{13} for $x = 0$, 1, 2, 3, 4 wt%, respectively. The variation of ε_r is non-monotonic, which can be due to heterogeneous mixing of Zn nanoparticles in CuTl-1223 matrix, but the overall suppression of dielectric properties may be due to reduction of defects after the addition of metallic Zn nanoparticles. The variation of maximum values of ε_r with Zn nanoparticle content in $(Zn)_x$/CuTl-1223 nanoparticle–superconductor composites is given in the inset of Fig. 6. The increase of maximum values of ε_r may be due to agglomeration and segregation of Zn nanoparticles in the bulk CuTl-1223 phase at higher concentration of Zn nanoparticles.

The variation in frequency-dependent real part of dielectric constant (ε') of these samples at room temperature is shown in Fig. 7. At lower frequency, dipolar polarization is dominant but when the frequency increases, the oscillation of the applied field increases and the dipolar polarization characteristic time becomes longer than the time constant of applied field. That is why decrease in ε' is observed. The maximum values of ε' at frequency 10^{-1} Hz are found around 1.32×10^9, 2.18×10^9, 2.16×10^8, 4.75×10^7, and 1.77×10^9 for $x = 0$, 1, 2, 3, 4 wt%, respectively. The variation of maximum values of ε' with Zn nanoparticle content in $(Zn)_x$/CuTl-1223 nanoparticle–superconductor composites is given in the inset of Fig. 7. The variation in frequency-dependent imaginary part of dielectric constant (ε'') of the samples at room temperature is shown in Fig. 8. All the investigated samples exhibit dielectric dispersion where decrease in ε'' is observed with the increase in frequency. The dielectric dispersion phenomenon has been explained on the basis of Maxwell–Wagner model of dielectrics [22,23],

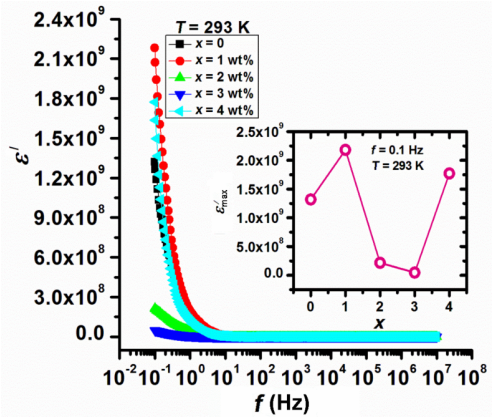

Fig. 7 Variation of real part of dielectric constant (ε') of $(Zn)_x$/CuTl-1223 nanoparticle–superconductor composites versus frequency for x = 0–4 wt%. In the inset, there are shown the variation of maximum ε' versus Zn nanoparticle content (i.e., x).

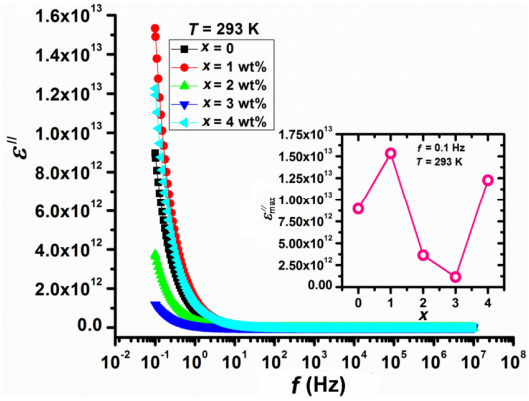

Fig. 8 Variation of imaginary part of dielectric constant (ε'') of $(Zn)_x$/CuTl-1223 nanoparticle–superconductor composites versus frequency for x = 0–4 wt%. In the inset, there are shown the variation of maximum ε'' versus Zn nanoparticle content (i.e., x).

according to which a dielectric medium is assumed to be made of well conducting grains separated by grain boundaries. At lower frequencies, the grain boundaries are more effective, due to which charges hop, resulting in higher dielectric constant. The decrease observed with increasing frequency is due to decrease in polarization as the dipoles do not have the capacity to follow the applied field at high frequencies. The maximum values of ε'' at frequency 10^{-1} Hz are found around 8.96×10^{12}, 1.53×10^{13}, 3.64×10^{12}, 1.15×10^{12}, and 1.23×10^{13} for $x=0$, 1, 2, 3, 4 wt%, respectively. The variation in frequency-dependent tangent loss ($\tan\delta$) of the samples at room temperature is shown in Fig. 9. The peaks appeared correspond to dispersion positions indicating the relaxation process. Maximum dissipation is observed because of relaxation time of electrical dipoles, which is near the applied electric field. The

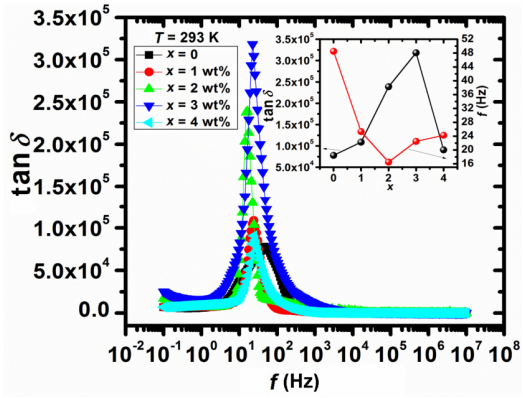

Fig. 9 Variation of dielectric loss factor ($\tan\delta$) of $(Zn)_x$/CuTl-1223 nanoparticle–superconductor composites with frequency for x = 0–4 wt%. In the inset, there are shown the variation of maximum $\tan\delta$ versus Zn nanoparticle content (i.e., x).

maximum values of $\tan\delta$ at frequency 10^{-1} Hz are found around 6.89×10^3, 7.03×10^3, 1.73×10^4, 2.49×10^4, and 6.92×10^3 for $x=0$, 1, 2, 3, 4 wt%, respectively. A decreasing trend in $\tan\delta$ is seen at low frequency, which is due to the effective grain boundaries. The peak in $\tan\delta$ can be observed at different frequencies with the addition of these Zn nanoparticles, which is 7.8×10^4 at 48.48 Hz, 1.09×10^5 at 24.25 Hz, 2.39×10^5 at 16.50 Hz, 3.18×10^5 at 22.45 Hz, and 9.08×10^4 at 24.25 Hz for the samples with $x=0$, 1, 2, 3, 4 wt%, respectively.

At relaxation frequency, the most apparent relaxation time, τ, is given by

$$\omega\tau = 1 \tag{7}$$

where ω is the angular frequency.

The variation in frequency-dependent ac-conductivity (σ_{ac}) of $(Zn)_x$/CuTl-1223 nanoparticle–superconductor composites at room temperature is shown in Fig. 10. Maximum values of σ_{ac} at frequency 10^7 Hz are found to be 0.69, 1.27, 0.21, 0.077, and 0.88 S/cm for $x=0$, 1, 2, 3, 4 wt%, respectively. The value of σ_{ac} increases as a whole after the addition of Zn nanoparticles in CuTl-1223 superconducting matrix. The possible reason for this increase in σ_{ac} is due to healing up of the micro-cracks, which results in the improvement of inter-grain connectivity. The ac-conductivity (σ_{ac}) of our samples increases at high frequencies, which happens due to bound carriers trapped in the samples. When ac-conductivity (σ_{ac}) decreases with increasing frequency, it happens due to the free carriers. In the inset, there is shown the variation of maximum value of σ_{ac} versus Zn nanoparticle content, showing a random trend in variation,

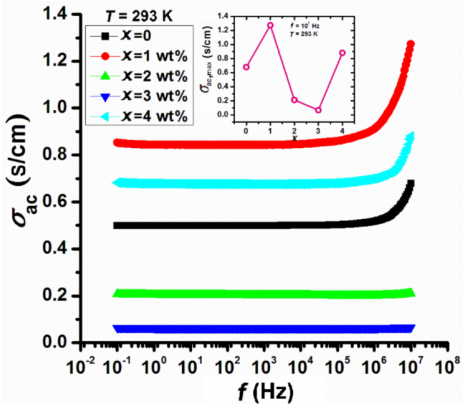

Fig. 10 Variation of ac-conductivity (σ_{ac}) of $(Zn)_x$/CuTl-1223 nanoparticle–superconductor composites with frequency for $x = 0$–4 wt%. In the inset, there is shown the variation of maximum σ_{ac} versus Zn nanoparticle content (i.e., x).

which may be due to inhomogeneous distribution of these nanoparticles in the CuTl-1223 matrix.

4 Conclusions

$(Zn)_x$/CuTl-1223 nanoparticle–superconductor composites were synthesized successfully by solid-state reaction method and characterized by different experimental techniques. Structural, morphological, compositional, superconducting, and dielectric properties were explored by XRD, SEM, EDX, and dielectric parameters of these composites. Granular structure with improved grain size could be observed by SEM micrographs. Tetragonal crystal structure of CuTl-1223 matrix was not altered after the addition of Zn nanoparticles, which provided evidence about their occupancy at the grain boundaries in the bulk CuTl-1223 material. The value of U was increased after the addition of Zn nanoparticles in CuTl-1223 composites. The improvement of superconducting properties could be accredited to the metallic nature of Zn nanoparticles, which could facilitate the mobility of carriers by improving the weak-links. Dielectric parameters have been decreased with the increase of frequency and became saturated at higher frequencies. The ac-conductivity (σ_{ac}) was seen to be increased non-monotonically due to heterogeneous distribution of Zn nanoparticles in CuTl-1223 matrix.

Acknowledgements

Higher Education Commission (HEC) of Pakistan is acknowledged for financial support through Project No. 20-1482/R&D/09-1472. Authors are also highly thankful to Prof. Xiang-Gang Qiu, Beijing National Laboratory of Condensed Matter Physics, Institute of Physics (IOP), Chinese Academy of Sciences (CAS), Beijing, China, for providing the characterization facilities.

References

[1] Yamamoto H, Tanaka K, Tokiwa K, *et al*. Synthesis of $Cu_{1-x}Tl_xBa_2Ca_2Cu_3O1_{1-y}$ (x~0.7) superconductor by hot press. *Physica C* 1998, **302**: 137–142.

[2] Awad R. Enhancement the formation of (Cu, Tl)-1223 superconducting phase by Cd-substitution. *J Alloys Compd* 2009, **474**: 517–521.

[3] Ihara H, Tanaka K, Tanaka Y, *et al.* Mechanism of T_c enhancement in $Cu_{1-x}Tl_x$-1234 and -1223 system with $T_c >$ 130 K. *Physica C* 2000, **341–348**: 487–488.

[4] Ihara H. How to achieve the best performance superconductor based on Cu-1234. *Physica C* 2001, **364–365**: 289–297.

[5] Tanaka K, Iyo A, Terada N, *et al.* Tl valence change and T_c enhancement (> 130 K) in $(Cu,Tl)Ba_2Ca_2Cu_3O_y$ due to nitrogen annealing. *Phys Rev B* 2001, **63**: 064508.

[6] Çavdar Ş, Koralay H, Tuğluoğlu N, *et al*. Frequency-dependent dielectric characteristics of Tl–Ba–Ca–Cu–O bulk superconductor. *Supercond Sci Technol* 2005, **18**: 1204.

[7] Mohammed NH. Effect of MgO nano-oxide additions on the superconductivity and dielectric properties of $Cu_{0.25}Tl_{0.75}Ba_2Ca_3Cu_4O_{12-\delta}$ superconducting phase. *J Supercond Nov Magn* 2012, **25**: 45–53.

[8] Nkum RK, Gyekye MO, Boakye F. Normal-state dielectric and transport properties of In-doped Bi–Pb–Sr–Ca–Cu–O. *Solid State Commun* 2002, **122**: 569–573.

[9] Younis A, Khan NA, Bajwa NU. Dielectric properties of $Cu_{0.5}Tl_{0.5}Ba_2Ca_3Cu_{4-y}Zn_yO_{12-\delta}$ ($y = 0$, 3) superconductors. *J Korean Phys Soc* 2010, **57**: 1437–1443.

[10] Mumtaz M, Khan NA, Khurram AA. Enhanced superconducting properties of $Cu_{0.5}(Tl_{0.5-y}Hg_y)Ba_2Ca_3Cu_4O_{12-\delta}$ ($y = 0$, 0.15, 0.25, 0.35) superconductor. *J Alloys Compd* 2008, **452**: 435–440.

[11] Khan NA, Husnain G, Sabeeh K. Enhanced superconductivity in $Cu_{0.5}Tl_{0.5}Ba_2Ca_{n-1-y}Be_yCu_nO_{2n+4-\delta}$ ($n = 3$, 4 and $y = 0.7$, 1.5, 1.7, 2.0) system with oxygen doping. *J Phys Chem Solids* 2006, **67**: 1841–1849.

[12] Ihara H, Tokiwa K, Tanaka K, *et al*. $Cu_{1-x}Tl_xBa_2Ca_3Cu_4O_{12-y}$ ($Cu_{1-x}Tl_x$-1234) superconductor with $T_c = 126$ K. *Physica C* 1997, **282–287**: 957–958.

[13] Ben-Ishai P, Sader E, Feldman Y, *et al*. Dielectric properties of $Na_{0.7}CoO_2$ and of the superconducting $Na_{0.3}CoO_2{\cdot}1.3H_2O$. *J Supercond* 2005, **18**: 455–459.

[14] Kamalasanan MN, Kumar ND, Chandra S. Dielectric and ferroelectric properties of $BaTiO_3$ thin films grown by the sol–gel process. *J Appl Phys* 1993, **74**: 5679.

[15] Xu X, Jiao Z, Fu M, *et al*. Dielectric studies in a layered Ba based Bi-2222 cuprate $Bi_2Ba_2Nd_{1.6}Ce_{0.4}Cu_2O_{10+\delta}$. *Physica C* 2005, **417**: 166–170.

[16] Çavdar Ş, Koralay H, Altındal Ş. Effect of vanadium substitution on the dielectric properties of glass ceramic Bi-2212 superconductor. *J Low Temp Phys* 2011, **164**: 102–114.

[17] Annabi M, Bouchoucha I, Azzouz FB, *et al*. Effect of ZnO and $Zn_{0.95}Mn_{0.05}O$ nano-particle inclusions on YBCO polycrystalline pinning properties. *IOP Conf Ser: Mater Sci Eng* 2010, **13**: 012009.

[18] Mumtaz M, Khan NA. Dielectric properties of $Cu_{0.5}Tl_{0.5}Ba_2Ca_3Cu_4O_{12-\delta}$ bulk superconductor. *Physica C* 2009, **469**: 728–731.

[19] Mumtaz M, Rahim M, Khan NA, *et al*. Dielectric properties of oxygen post-annealed $Cu_{0.5}Tl_{0.5}Ba_2Ca_3(Cu_{4-y}Cd_y)O_{12-\delta}$ bulk superconductor. *Ceram Int* 2013, **39**: 9591–9598.

[20] Abdeen W, Mohammed NH, Awad R, *et al.* Influence of nano-Ag addition on phase formation and electrical properties of $(Cu_{0.5}Tl_{0.5})$-1223 superconducting phase. *J Supercond Nov Magn* 2013, **26**: 623–631.

[21] Jabbar A, Mumtaz M, Nadeem K. Noble metals (Ag, Au) nanoparticles addition effects on superconducting properties of CuTl-1223 phase. *Eur Phys J Appl Phys* 2015, **69**: 30601.

[22] Wagner KW. Zur Theorie der unvollkommenen Dielektrika. *Annalen der Physik* 1913, **345**: 817–855.

[23] Tselev A, Brooks CM, Anlage SM, *et al*. Evidence for power-law frequency dependence of intrinsic dielectric response in the $CaCu_3Ti_4O_{12}$. *Phys Rev B* 2004, **70**: 144101.